

Exact and asymptotic computations of elementary spin networks: classification of the quantum–classical boundaries (\ddagger)

A.C.P. Bitencourt⁽¹⁾, A. Marzuoli⁽²⁾, M. Ragni⁽³⁾, R.W. Anderson⁽⁴⁾
and V. Aquilanti⁽⁵⁾

(1) Centro de Ciências Exatas e Tecnológicas, Universidade Federal do Recôncavo da Bahia, Cruz das Almas, Bahia (BR); (2) Dipartimento di Matematica ‘F Casorati’, Università degli Studi di Pavia and INFN, Sezione di Pavia, 27100 Pavia (IT); (3) Departamento de Física, Universidade Estadual de Feira de Santana, Feira de Santana, Bahia (BR); (4) Department of Chemistry, University of California, Santa Cruz, California (USA); (5) Dipartimento di Chimica, Università degli Studi di Perugia, 06123 Perugia (IT)

Abstract

Increasing interest is being dedicated in the last few years to the issues of exact computations and asymptotics of spin networks. The large–entries regimes (semiclassical limits) occur in many areas of physics and chemistry, and in particular in discretization algorithms of applied quantum mechanics. Here we extend recent work on the basic building block of spin networks, namely the Wigner $6j$ symbol or Racah coefficient, enlightening the insight gained by exploiting its self–dual properties and studying it as a function of two (discrete) variables. This arises from its original definition as an (orthogonal) angular momentum recoupling matrix. Progress also derives from recognizing its role in the foundation of the modern theory of classical orthogonal polynomials, as extended to include discrete variables. Features of the imaging of various regimes of these orthonormal matrices are made explicit by computational advances –based on traditional and new recurrence relations– which allow an interpretation of the observed behaviors in terms of an underlying Hamiltonian formulation as well. This paper provides a contribution to the understanding of the transition between two extreme modes of the $6j$, corresponding to the nearly classical and the fully quantum regimes, by studying the boundary lines (caustics) in the plane of the two matrix labels. This analysis marks the evolution of the turning points of relevance for the semiclassical regimes and puts on stage an unexpected key role of the Regge symmetries of the $6j$.

(\ddagger) Talk presented at ICCSA 2012 [12th International Conference on Computational Science and Applications, Salvador de Bahia (Brazil) June 18–21, 2012], Lecture Notes in Computer Science **7333**, Part I, pp 723–737 (Murgante B. et al. Eds.) Springer-Verlag, Berlin-Heidelberg 2012 ISBN 978-3-642-31124-6

1 Introduction

This is an account of progress on understanding elementary spin networks in view of their ubiquitous occurrence in applications far beyond the theory of angular momentum in quantum mechanics where they were introduced by Wigner, Racah and others. They have been (and are) precious tools for computational nuclear, atomic, molecular and chemical physics: best known examples are vector coupling and recoupling coefficients and $3nj$ symbols [1, 2, 3, 4, 5, 6, 7, 8, 9, 10, 11, 12, 13, 14, 15].

The diagrammatic tools for “spin networks” were developed by the Yutsis school and by others [16, 17], and were given this collective name in connection with applications to discretized models for quantum gravity after Penrose [18], Ponzano and Regge [19], and many others (see *e.g.* [20, 21]).

The basic building blocks of (all) spin networks are the Wigner $6j$ symbols or Racah coefficients, which we are study here by exploiting their self dual properties and consequently looking at them as functions of two variables. This approach is most natural in view of their origin as matrix elements describing recoupling between alternative angular momentum binary coupling schemes, or between alternative hyperspherical harmonics, or between alternative atomic and molecular orbitals, *etc.*, and utilizes progress in understanding their role in the foundation of the modern theory of classical orthogonal polynomials, as extended to include discrete variables [22]. Features of the imaging of the orthonormal matrices is made possible by computational advances, that permit to elaborate accurate illustrations and comparisons, using exact computations based on traditional and new recurrence relations, which allow in turn an interpretation of the observed behaviors in terms of an underlying Hamiltonian formulation. An unexpected key role of the (mysterious) Regge symmetries [23] of the $6j$ is briefly discussed. Suitable use of the results for discretization algorithms of applied quantum mechanics is stressed, with particular attention to problems arising in atomic and molecular physics.

For background information and notation, we will refer to our previous papers [7, 9, 11], regarding the one dimensional view, and also to [24, 25], where ample attention is devoted to the two dimensional perspective and where the related $4j$ model is elaborated in great detail.

2 Background information

Semiclassical and asymptotic views are introduced to describe the dependence on parameters. They originated from the early association due to Racah and Wigner to geometrical features, respectively a dihedral angle and the volume of an associated tetrahedron (see Fig. 4 in [11]), which is the starting point of the seminal paper by Ponzano and Regge [19]. Their results provided an impressive insight into the functional dependence of angular momentum functions showing a quantum mechanical picture in terms of formulas which describe classical and non-classical discrete wavelike regimes, as well as the transition between them.

The symmetries with respect to exchange of role of the matrix entries of the $6j$ (transpositions), easily understood also from the associated tetrahedron picture, are well characterized. Similarly, we find that the mirror symmetries can be exploited when the symbols are employed in applications beyond angular momentum theory, implying meaning of the entries as quantities that can have a sign.

From the detailed study of combinatorial properties (requiring only triangular relationships associated to angular momentum coupling, and the closure quadrilateral property associated to coupling of four angular momenta), it emerged very recently [24] how to uniquely assign labels to the elements of the grids for the matrix for which the orthonormalized Racah–Wigner coefficients are the elements. Figures of zero volume and ridges are among properties that can be monitored on such square “screen”: we sketch relationships and concept of Regge twins, “canonical” form and simplification of the following due to a suitable chosen ordering. From a computational viewpoint, explicit formulas are available as sums over a single variable. However, resorting to recursion formulas appears most convenient for exact calculations. Also, we will exploit them for semi–classical analysis, both to understand the high j –limit and, in reverse, to interpret the symbols them as discrete wave–functions obeying Schrödinger type of difference (rather than differential) equations. We have derived and computationally implemented a two–variable recurrence that permits construction of the whole orthonormal matrix. The derivation follows our paper in [10] and is of interest also for other $3nj$ symbols in general. Separation of the two–variable recurrence relation leads to the basic three–term recurrence as depending on a single variable. It can be shown that it can be re–derived also from the Biedenharn–Elliot relationship in a form that shows the connection to a Schrödinger type of equation in the Hamiltonian formulation (for alternative Lagrangian formulations, see [25]). The following analysis of the caustics (and of the ridge curves, see below) is intended to characterize the modes of the spin network, as well as the guiding principles of the asymptotic analysis.

3 The screen: mirror, Piero and Regge symmetries

Following e.g. the Schulten and Gordon approach [26], in [27] it is shown that the $6j$ symbol becomes the eigenfunction of the Schrödinger–like equation in the variable q , a continuous generalization of j_{12} :

$$\left[\frac{d}{dq^2} + p^2(q) \right] \Psi(q) = 0, \quad (1)$$

where $\Psi(q)$ is related to

$$\left\{ \begin{array}{ccc} j_1 & j_2 & j_{12} \\ j_3 & j & j_{23} \end{array} \right\} \quad (2)$$

and p^2 is related with the square of the volume V of the associated tetrahedron (Fig 4 in [11]), whose edges are considered continuous and given by $J_1 = j_1 + 1/2$, $J_2 = j_2 + 1/2$, $J_{12} = j_{12} + 1/2$, $J_3 = j_3 + 1/2$, $J = j + 1/2$, and $J_{23} = j_{23} + 1/2$. The Cayley–Menger determinant permits to calculate the square of the volume of a generic tetrahedron in terms of (squares of) its edge lengths according to

$$V^2 = \frac{1}{288} \begin{vmatrix} 0 & J_3^2 & J^2 & J_{23}^2 & 1 \\ J_3^2 & 0 & J_{12}^2 & J_2^2 & 1 \\ J^2 & J_{12}^2 & 0 & J_1^2 & 1 \\ J_{23}^2 & J_2^2 & J_1^2 & 0 & 1 \\ 1 & 1 & 1 & 1 & 0 \end{vmatrix}. \quad (3)$$

The condition for the tetrahedron with fixed edge lengths to exist as a polyhedron in Euclidean 3-space amounts to require $V^2 > 0$, while the $V^2 = 0$ and $V^2 < 0$ cases were associated by Ponzano and Regge to “flat” and nonclassical tetrahedral

configurations respectively. Equivalent to (3) is the Gramian determinant, used in [24] and [25], which embodies a clearer relationship with a vectorial picture.

Major insight is provided by plotting both $6j$ s and geometrical functions (volumes, products of face areas, *etc.*) of the associated tetrahedra in a 2-dimensional $j_{12} - j_{23}$ plane (the square “screen” of allowed ranges of j_{12} and j_{23} to be used in all the pictures below). Actually both (3) and the Gramian are equivalent to the famous formula known to Euler but first found five centuries ago by the Renaissance mathematician, architect and painter Piero della Francesca. The formulas of course embody all the well known “classical” symmetries of geometrical tetrahedra, which show up in the $6j$ symbol as well on applying concerted interchanges of its entries. Non-obvious symmetries of particular relevance in what follows are listed below.

- (i) *The mirror symmetry.* The appearance of squares of tetrahedron edges entails that the invariance with respect to the exchange $J \leftrightarrow -J$ implies formally $j \leftrightarrow -j - 1$ with respect to the entries of the $6j$ symbol. Although this is physically irrelevant when the j s are pseudo-vectors, such as physical spins or orbital angular momenta, it can be of interest for other (*e.g.* discrete algorithms) applications. Regarding the screen, it can be seen that actually by continuation of the abscissa $x = J_{12}$ and ordinate $y = J_{23}$ to negative values, one can have replicas that can be glued by cutting out regions shaded in [9]. This allows mapping of the screen to the S^2 phase space found in [25].
- (ii) *Piero line.* In general, an exchange of opposite edges of a tetrahedron (or of the two entries in a column in the $6j$ symbol) corresponds to different tetrahedra and different symbols. In Piero formula, there is a term due to this difference that vanishes when any pair of opposite edges are equal. In general, a line can be drawn on the screen when ranges of j_{12} and j_{23} overlap and in the screen one may encounter what we call a Piero line: when two entries in a column are equal, this line is a diagonal corresponding to the exchange $x \leftrightarrow y$. Then, images on the screen will be symmetric with respect to such a line, as shown below with explicit examples.
- (iii) *Regge symmetries.* The manifestation of these intriguing symmetries in the present context is of paramount interest: it might be elucidated through connection with the projective geometry of the elementary quantum of space, which is being reconsidered from the viewpoint of association to the polygonal inequalities (triangular and quadrilateral in the $6j$ case), which have to be enforced in any spin networks. We find insightful to exhibit the basic Regge symmetry [23] in the following form

$$\begin{aligned} \left\{ \begin{array}{ccc} j_1 & j_2 & j_{12} \\ j_3 & j & j_{23} \end{array} \right\} &= \left\{ \begin{array}{ccc} (j_1 + j_2 - j_3 + j)/2 & (j_1 + j_2 + j_3 - j)/2 & j_{12} \\ (-j_1 + j_2 + j_3 + j)/2 & (j_1 - j_2 + j_3 + j)/2 & j_{23} \end{array} \right\} \\ &= \left\{ \begin{array}{ccc} j_1 + \rho & j_2 - \rho & j_{12} \\ j_3 + \rho & j - \rho & j_{23} \end{array} \right\}, \end{aligned} \quad (4)$$

where $\rho = (-j_1 + j_2 - j_3 - j)/2 = [(j_2 + j) - (j_1 + j_3)]/2$. Often the Regge symmetry is written in terms of the semi-perimeter $s = (j_1 + j_2 + j_3 + j)/2$. Obviously, $s = \rho + j_1 + j_3 = -\rho + j_2 + j$.

The key observation is made in [25] that the range of both J_{12} and J_{23} , namely the “size” of the screen, is given by $2\min\{J_1, J_2, J_3, J, J_1 + \rho, J_2 + \rho, J_3 + \rho, J + \rho\}$.

Therefore, for definiteness and no loss of generality, we are allowed in most cases to conveniently choose for the discussion whichever of the two j symbols twinned by (4) contains such a minimum value.

4 Features of the tetrahedron volume function

Looking at the volume V as a function of $x = J_{12}$ and $y = J_{23}$, and after some algebraic manipulations, we get the expressions for the x_{Vmax} and y_{Vmax} that correspond to the maximum of the volume for a fixed value of x or y (respectively), namely

$$x_{Vmax}^2 = \frac{A(J, J_2) + J_t^2 y^2 - y^4}{2 y^2}, \quad (5)$$

$$y_{Vmax}^2 = \frac{A(J_2, J) + J_t^2 x^2 - x^4}{2 x^2}, \quad (6)$$

where

$$\begin{aligned} A(a, b) &= (J_1 + a)(J_1 - a)(J_3 + b)(J_3 - b), \\ J_t^2 &= J_1^2 + J_2^2 + J_3^2 + J^2. \end{aligned} \quad (7)$$

We call ‘‘ridge’’ curves the plots of Eqs. (5) and (6) on the x, y -screen. Each one marks configurations of the associated tetrahedron when two specific pairs of triangular faces are orthogonal. The corresponding values of the volume ($V_{max,x}$ and $V_{max,y}$) are

$$V_{max,x} = \frac{2 F(J_1, J, y) F(J_2, J_3, y)}{3 y}, \quad (8)$$

$$V_{max,y} = \frac{2 F(J_1, J_2, x) F(J, J_3, x)}{3 x}, \quad (9)$$

where

$$F(a, b, c) = \frac{\sqrt{(a+b+c)(a+b-c)(a-b+c)(-a+b+c)}}{4}, \quad (10)$$

is the area of the triangle with sides a, b and c .

Curves corresponding to $V = 0$ (the caustic curves) obey the equations

$$\begin{aligned} x_z^2 &= x_{Vmax}^2 \pm \frac{12 V_{max,x}}{y}, \\ y_z^2 &= y_{Vmax}^2 \pm \frac{12 V_{max,y}}{x}, \end{aligned} \quad (11)$$

Figure 1(a) shows these curves for the $\left\{ \begin{array}{ccc} 45 & 30 & j_{12} \\ 55 & 60 & j_{23} \end{array} \right\}$ case. The inside region enclosed by the ovaloid is that of finite volume tetrahedra, the ovaloids themselves correspond to configurations of flattened tetrahedra, specifically convex planar quadrilaterals at the upper right corner, concave planar quadrilaterals at both the upper left and the lower right corners, and crossed planar quadrilaterals at the lower left corner.

For particular values of j_1, j_2, j_3 and j linear configurations are allowed as well. These interesting degenerate cases are illustrated in the other panels of Fig. 1. In Fig. 1(b) the case of $j_1 + j = j_2 + j_3$ is considered. The other interesting cases are obtained for $j_1 + j_2 = j_3 + j$ (Fig. 1(c)) and for $j_1 + j_3 = j_2 + j$ (Fig. 1(d)).

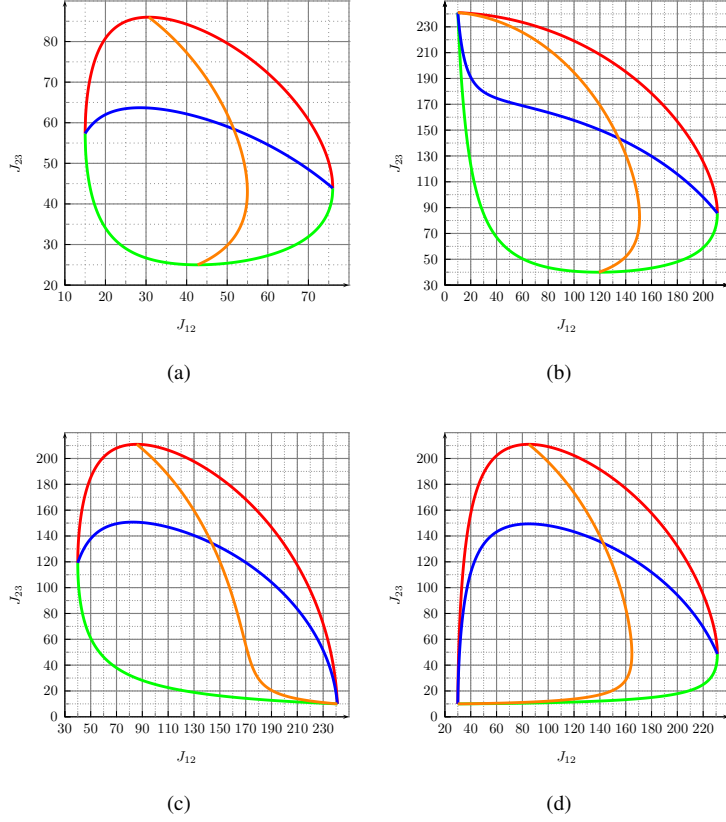


Figure 1: Plots of the caustics and ridges given by Eqs.(5-11) for four sets of $6j$ -symbols. Panel 1(a), $j_1 = 45, j_2 = 30, j_3 = 55$ and $j = 60$. $15 \leq J_{12} \leq 76$ and $25 \leq J_{23} \leq 86$. Panel 1(b), $j_1 = 140, j_2 = 130, j_3 = 110$ and $j = 100$. $10 \leq J_{12} \leq 211$ and $40 \leq J_{23} \leq 241$. Panel 1(c), $j_1 = 140, j_2 = 100, j_3 = 110$ and $j = 130$. $40 \leq J_{12} \leq 241$ and $10 \leq J_{23} \leq 211$. Panel 1(d), $j_1 = 140, j_2 = 110, j_3 = 100$ and $j = 130$. $30 \leq J_{12} \leq 231$ and $10 \leq J_{23} \leq 211$.

Note that, due to the symmetry properties of the $6j$ symbols, the cases $j_1 + j = j_2 + j_3$ and $j_1 + j_2 = j_3 + j$ are intrinsically equivalent. Figure 1(d) shows the effect of degeneracy with respect to the far from obvious Regge symmetry, which manifests as specularity with respect to the Piero line, in this case the diagonal from the origin in the square screen.

5 Symmetric and limiting cases

When some or all the j 's are equal, interesting features appear in the screen. Similarly when some are larger than others.

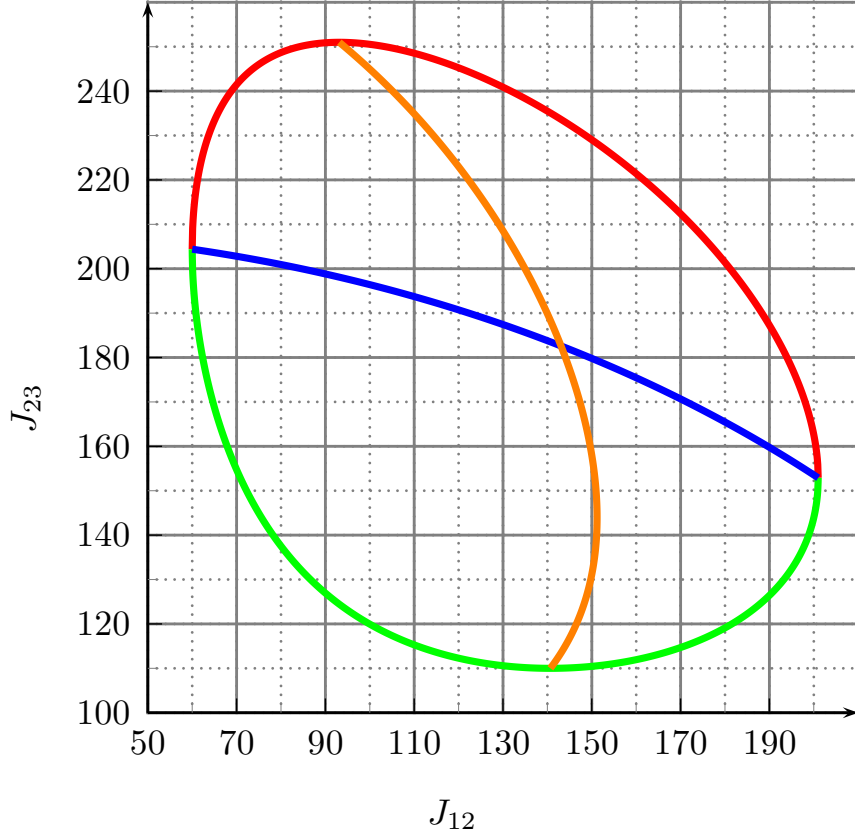


Figure 2: Plots of the caustics and ridges (Eqs.5-11) for the $6j$ -symbols with $j_1 = 100$, $j_2 = 100$, $j_3 = 150$ and $j = 210$. $60 \leq J_{12} \leq 201$ and $110 \leq J_{23} \leq 251$.

5.1 Symmetric cases

For $j_1 = j_2$ plots of Eqs.(5-11) like those of Fig. 2 are obtained (equivalent to the $j_3 = j$ one, in virtue of standard symmetries).

For $j_1 = j_3$ plots of Eqs.(5-11) like that of Fig. 3 are obtained. For symmetry this case is equivalent to the $j_2 = j$ one.

Imposing both $j_1 + j = j_2 + j_3$ and $j_1 + j_2 = j_3 + j$ we have that $j_1 = j_3$ and $j_2 = j$. See Figs. 4(a) e 4(b).

Imposing both $j_1 + j = j_2 + j_3$ and $j_1 + j_3 = j_2 + j$ we have that $j_1 = j_2$ and $j_3 = j$. In these conditions, plots of Eqs.(5-11) like those of Fig. 5 are obtained.

This case is formally equivalent to the one where $j_1 = j$ and $j_3 = j_2$ which is obtained imposing $j_1 + j_2 = j_3 + j$ and $j_1 + j_3 = j_2 + j$.

5.2 Limiting cases

Interestingly, the Fig. 5 permits us to discuss the caustics of the $3j$ symbols as limiting case of the corresponding $6j$ where three entries are larger than the other ones, namely:

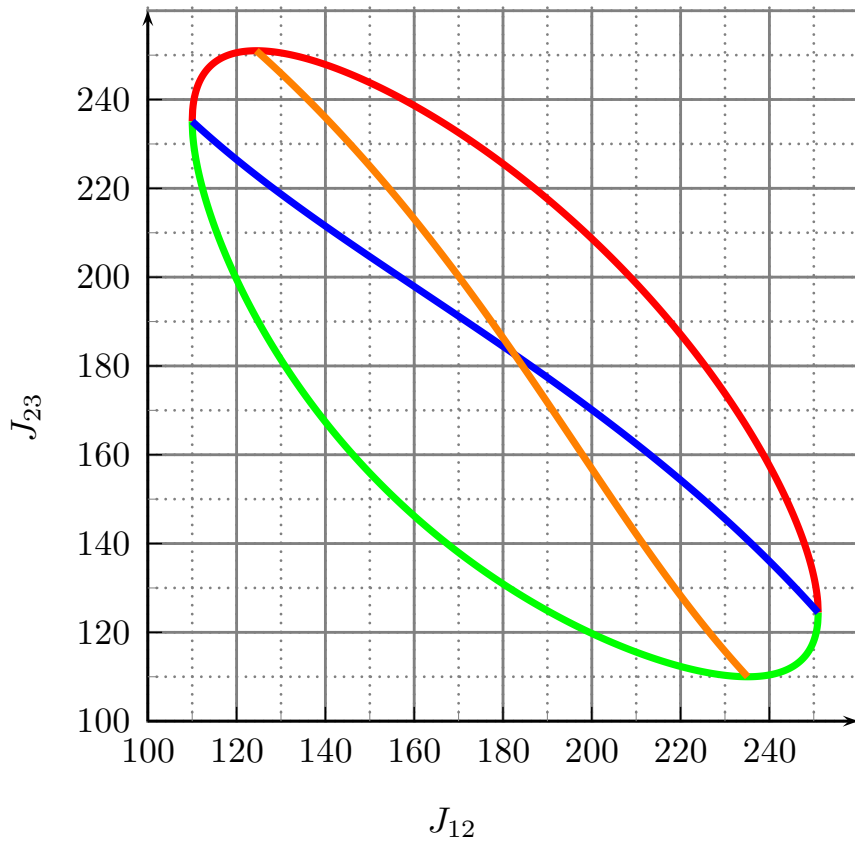


Figure 3: Plots of the caustics and ridges (Eqs.5-11) for the $6j$ -symbols with $j_1 = 100$, $j_2 = 150$, $j_3 = 100$ and $j = 210$. $110 \leq J_{12} \leq 251$ and $110 \leq J_{23} \leq 251$.

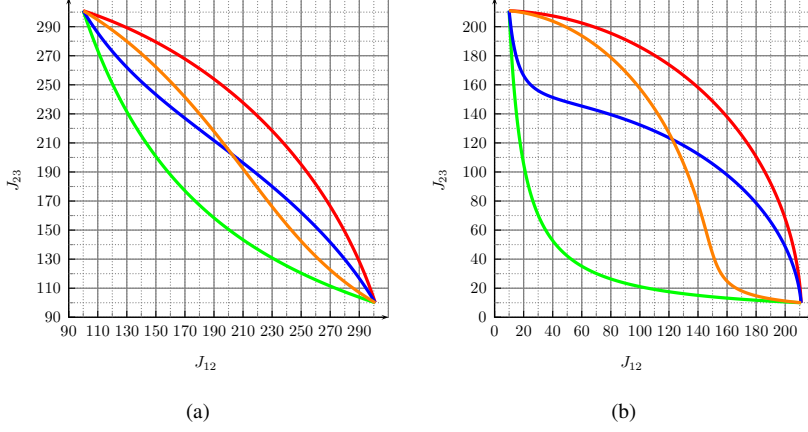


Figure 4: Plots of the caustics and ridges (Eqs.5-11) for two sets of $6j$ symbols. Panel 4(a), $j_1 = 200, j_2 = 100, j_3 = 200$ and $j = 100$. $100 \leq J_{12} \leq 301$ and $100 \leq J_{23} \leq 301$. Panel 4(b), $j_1 = 110, j_2 = 100, j_3 = 110$ and $j = 100$. $10 \leq J_{12} \leq 211$ and $10 \leq J_{23} \leq 211$.

$$\begin{pmatrix} j_1 & j_2 & j_3 \\ m_1 & m_2 & m_3 \end{pmatrix} = \lim_{R \rightarrow \infty} \left\{ \begin{matrix} j_1 & j_2 & j_3 \\ l_1 + R & l_2 + R & l_3 + R \end{matrix} \right\}, \quad (12)$$

where

$$\begin{aligned} m_1 &= l_3 - l_2, \\ m_2 &= l_1 - l_3. \end{aligned} \quad (13)$$

If we define

$$\begin{aligned} m_1 &:= F + D, \\ m_2 &:= F - D, \\ \bar{R} &:= R + l_3 - D, \end{aligned} \quad (14)$$

we have

$$\begin{pmatrix} j_1 & j_2 & j_3 \\ m_1 & m_2 & m_3 \end{pmatrix} = \lim_{\bar{R} \rightarrow \infty} \left\{ \begin{matrix} j_1 & j_2 & j_3 \\ \bar{R} + F & \bar{R} - F & \bar{R} + D \end{matrix} \right\}. \quad (15)$$

For $\bar{R} \rightarrow \infty$ it is $\bar{R} \pm F \simeq \bar{R}$.

The caustic of the $3j$ symbol is defined as

$$\begin{vmatrix} 0 & J_1^2 - m_1^2 & J_2^2 - m_2^2 & 1 \\ J_1^2 - m_1^2 & 0 & J_3^2 - m_3^2 & 1 \\ J_2^2 - m_2^2 & J_3^2 - m_3^2 & 0 & 1 \\ 1 & 1 & 1 & 0 \end{vmatrix} = 0, \quad (16)$$

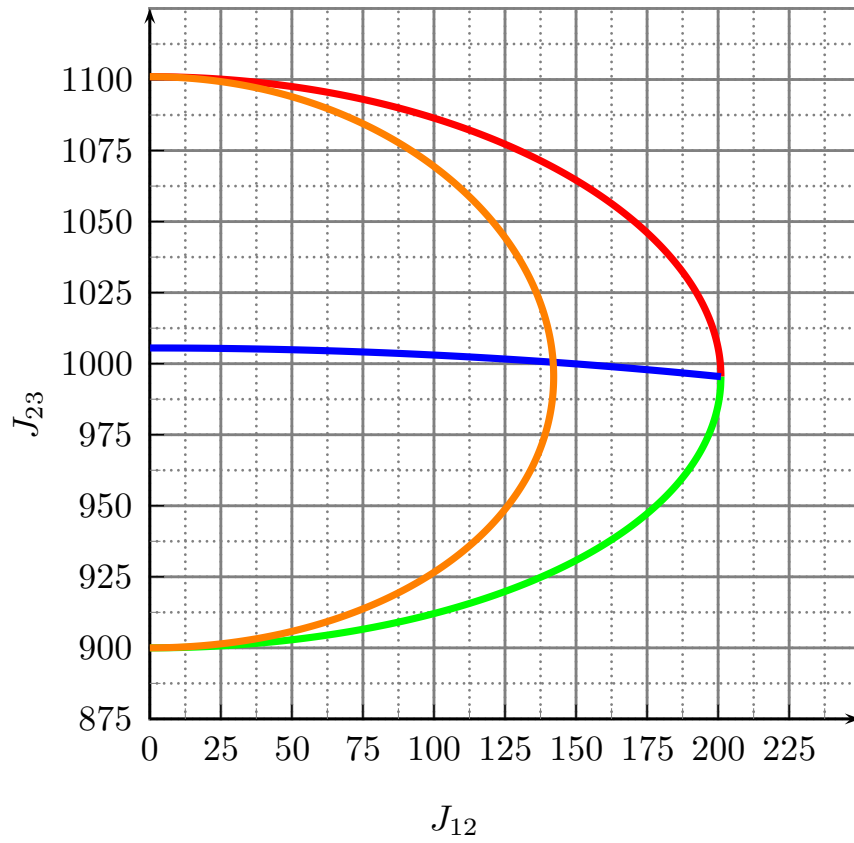


Figure 5: Plots of the caustics and ridges (Eqs.5-11) for the $6j$ symbols with $j_1 = 1000$, $j_2 = 1000$, $j_3 = 100$ and $j = 100$. $0 \leq J_{12} \leq 201$ and $900 \leq J_{23} \leq 1001$. According to the text, this figure also exemplifies features of ridges and caustics for a $3j$ symbol.

and

$$\left| \begin{array}{cccc} 0 & J_1^2 - m_1^2 & J_2^2 - m_2^2 & 1 \\ J_1^2 - m_1^2 & 0 & J_3^2 - m_3^2 & 1 \\ J_2^2 - m_2^2 & J_3^2 - m_3^2 & 0 & 1 \\ 1 & 1 & 1 & 0 \end{array} \right| = \lim_{R \rightarrow \infty} \frac{\left| \begin{array}{cccc} 0 & (L_1 + R)^2 & (L_2 + R)^2 & (L_3 + R)^2 \\ (L_1 + R)^2 & 0 & J_3^2 & J_2^2 \\ (L_2 + R)^2 & J_3^2 & 0 & J_1^2 \\ (L_3 + R)^2 & J_2^2 & J_1^2 & 0 \\ 1 & 1 & 1 & 1 \end{array} \right|}{2R^2}, \quad (17)$$

The case of caustics on the screen for four large entries, leading to reduced Wigner d matrices, is studied in [8].

For $j_1 = j_2 = j_3 = j$ plots of Eqs.(5-11) like those of Fig. 6 are obtained. This case is obtained when $j_1 + j = j_2 + j_3$, $j_1 + j_2 = j_3 + j$ and $j_1 + j_3 = j_2 + j$.

Fig. 7 shows the caustics of a full-symmetric $6j$ when the symmetry is broken by varying j .

6 Remarks and Conclusion

Explicit computational formulas are available either as sums over a single variable and series. However recourse to recursion formulas appears most convenient for both exact calculations and -as we will emphasize- also for semiclassical analysis, in order to understand high j limits and in reverse to interpret them as discrete wavefunctions obeying Schrödinger type of difference (rather than differential) equations. In further work, we derive and computationally implement the two variable recurrence that permits construction of the whole orthonormal matrix. The derivation follows our paper in [10] and is of interest also for other $3nj$ symbols in general.

The extensive images of the exactly calculated $6j$'s on the square screens illustrate how the caustic curves studied in this paper separate the classical and nonclassical regions, where they show wavelike and evanescent behaviour respectively. Limiting cases, and in particular those referring to $3j$ and Wigner's d matrix elements can be analogously depicted and discussed. Interesting also are the ridge lines, which separate the images in the screen tending to qualitatively different flattening of the quadrilateral, namely convex in the upper right region, concave in the upper left and lower right ones, and crossed in the lower left region.

Interestingly, the Regge symmetries not only restrict the range of the discrete manifold, but also allow an assignment of the involved modes.

As a continuation of our recent work, this paper has demonstrated that interesting insight into properties of the basic building blocks of spin networks, the Wigner $6j$ symbols or Racah coefficients, is gained by exploiting their self dual properties and studying them as a function of two variables, an approach most natural in view of their origin as matrix elements. Features of their imaging of the orthonormal matrices are fostered by computational advances, which is being developed on traditional and new recurrence relations, which also allow interpretation of the underlying Hamiltonian mechanics: the borderline of the two limiting modes -quasi-classical and deeply quantum- has been the object of this paper. The characteristic features of this boundary line, described by the caustic curves which follow the turning points of the classical motion, have been elucidated. A key role was also revealed of the surprising Regge symmetries.

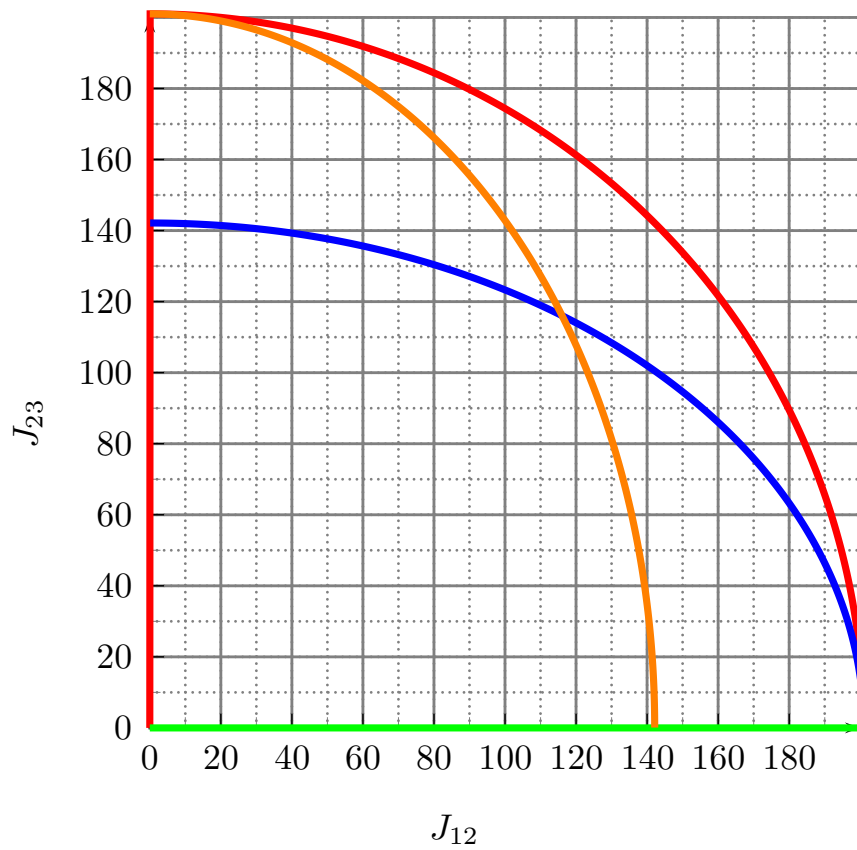


Figure 6: Plots of the caustics and ridges (Eqs.5-11) for the full symmetric $6j$ -symbols with $j_1 = 100$, $j_2 = 100$, $j_3 = 100$ and $j = 100$. $0 \leq J_{12}, J_{23} \leq 201$. This figure clearly points out the interest of extending the screen by mirror symmetries.

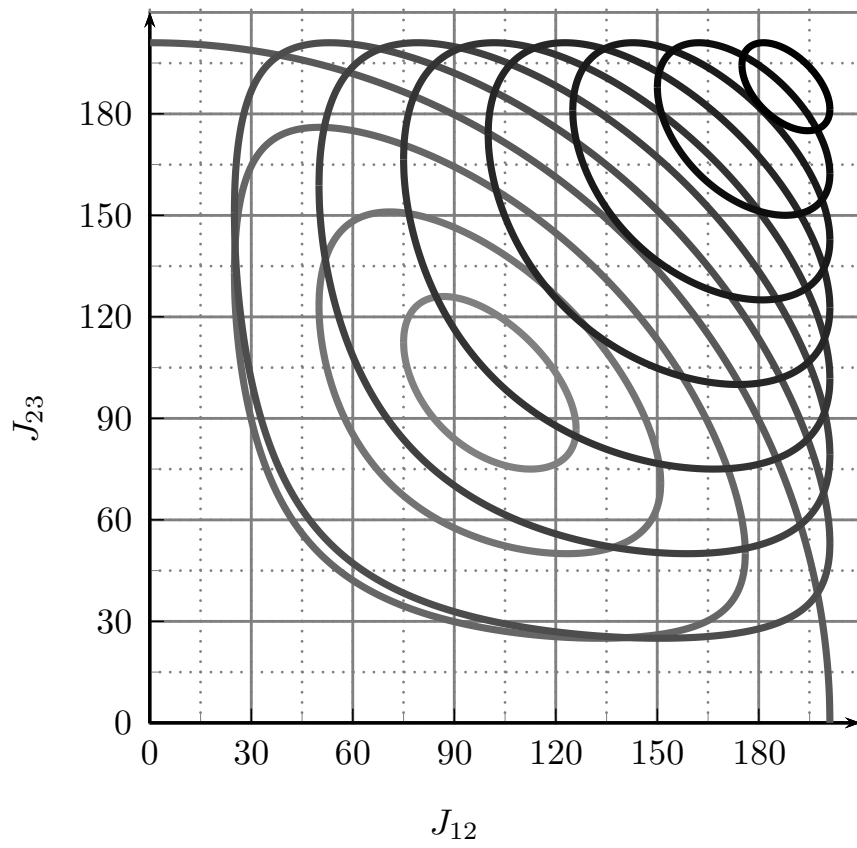


Figure 7: Plots of the caustics and ridges (Eqs.5-11) for $j_1 = j_2 = j_3 = 100$ while j varies from 25 (light line) to 275 (dark line) with step of 25 units.

Further work based on these tools involves detailed studies of some of the important aspects considered too briefly or not at all in this paper, such as the classical, mirror and Regge symmetries, the limiting cases to the simpler $3j$ coefficients and rotation matrix elements, the extensions to higher $3nj$ symbols and to the so called q deformations.

Semiclassical and asymptotic analysis provide limiting relationships converging into the Askey scheme. Relationships also arose then with orthogonal polynomials, and indicate avenues to views to generalizations (continuous extensions, relationships with harmonics of rotation groups, and finally q -extensions, ...). All these extensions may need some modifications when detailed properties are discussed, but in general studying $6j$ symbols continues to deserve further work.

Use is finally pointed out for discretization algorithms of applied quantum mechanics, particular attention being devoted to problems encountered in atomic and molecular physics.

Acknowledgments

MR and ACPB acknowledge the CNPq agency for the financial support. MR is also grateful for the financial support by the FAPESB agency.

References

- [1] V. Aquilanti, S. Cavalli, and G. Grossi, "Hund's cases for rotating diatomic molecules and for atomic collisions: angular momentum coupling schemes and orbital alignment," *Z. Phys. D.*, vol. 36, pp. 215–219 (1996).
- [2] V. Aquilanti and G. Capecchi, "Harmonic analysis and discrete polynomials. From semiclassical angular momentum theory to the hyperquantization algorithm," *Theor. Chem. Accounts*, vol. 104, pp. 183–188 (2000).
- [3] V. Aquilanti, S. Cavalli, and C. Coletti, "Angular and hyperangular momentum recoupling, harmonic superposition and Racah polynomials. a recursive algorithm," *Chem Phys. Letters*, vol. 344, pp. 587–600 (2001).
- [4] V. Aquilanti and C. Coletti, " $3nj$ -symbols and harmonic superposition coefficients: an icosahedral abacus," *Chem. Phys. Letters*, vol. 344, pp. 601–611 (2001).
- [5] D. De Fazio, S. Cavalli, and V. Aquilanti, "Orthogonal polynomials of a discrete variable as expansion basis sets in quantum mechanics. The hyperquantization algorithm," *Int. J. Quantum Chem.*, vol. 93, pp. 91–111 (2003).
- [6] V. Aquilanti, H. Haggard, R. Littlejohn, and L. Yu, "Semiclassical analysis of Wigner $3j$ -symbol," *J. Phys. A*, vol. 40, pp. 5637–5674 (2007).
- [7] V. Aquilanti, A.C.P. Bitencourt, C. da S. Ferreira, A. Marzuoli, and M. Ragni, "Quantum and semiclassical spin networks: from atomic and molecular physics to quantum computing and gravity," *Physica Scripta*, vol. 78, no. 058103 (7 pages) (2008).
- [8] R.W. Anderson, V. Aquilanti, and C. da S. Ferreira, "Exact computation and large angular momentum asymptotics of $3nj$ symbols: semiclassical disentangling of spin-networks," *J. Chem. Phys.*, vol. 129, no. 161101 (5 pages) (2008).
- [9] V. Aquilanti, A.C.P. Bitencourt, C. da S. Ferreira, A. Marzuoli, and M. Ragni, "Combinatorics of angular momentum recoupling theory: spin networks, their asymptotics and applications," *Theor. Chem. Accounts*, vol. 123, p. 237–247 (2009).
- [10] R.W. Anderson, V. Aquilanti, and A. Marzuoli, " $3nj$ morphogenesis and semiclassical disentangling," *J. Phys Chem A*, vol. 113, pp. 15106–15117 (2009).
- [11] M. Ragni, A.C.P. Bitencourt, C. da S. Ferreira, V. Aquilanti, R.W. Anderson, and R. Littlejohn, "Exact computation and asymptotic approximation of $6j$ symbols. illustration of their semiclassical limits," *Int. J. Quantum Chem.*, vol. 110, pp. 731–742 (2010).
- [12] V. Aquilanti, H. Haggard, A. Hedeman, N. Jeevanjee, R. Littlejohn, and L. Yu, "Semiclassical mechanics of the Wigner $6j$ -symbol," *J. Phys. A*, vol. 45, no. 065209 (2012).
- [13] V. Aquilanti, S. Cavalli, and D. De Fazio, "Angular and hyperangular momentum coupling coefficients as hahn polynomials," *J. Phys. Chem.*, vol. 99, pp. 15694–15698 (1995).

- [14] —, “Hyperquantization algorithm I. Theory for triatomic systems,” *J. Phys. Chem.*, vol. 109, pp. 3792 – 3805 (1998).
- [15] V. Aquilanti, S. Cavalli, D. De Fazio, and A. Volpi, “The A+BC reaction by the hyperquantization algorithm: the symmetric hyperspherical parametrization for $j > 0$,” *J. Phys. Chem.*, vol. 39, pp. 103 – 121 (2001).
- [16] A. Yutsis, I. Levinson, and V. Vanagas, *The Mathematical Apparatus of the Theory of Angular Momentum*. Jerusalem, Israel. Program for Sci. Transl. Ltd. (1962).
- [17] D. Varshalovich, A. Moskalev, and V. Khersonskii, *Quantum Theory of Angular Momentum*. Singapore, World Scientific (1988).
- [18] R. Penrose, “Angular momentum: an approach to combinatorial space–time,” *Quantum Theory and Beyond*. T. Bastin (Ed.), Cambridge Univ. Press (1971).
- [19] G. Ponzano and T. Regge, “Semiclassical limit of Racah coefficients,” *Spectroscopic and Group Theoretical Methods in Physics* (1968).
- [20] C. Rovelli, *Quantum Gravity*. Cambridge University Press (2004).
- [21] M. Carfora, A. Marzuoli, and M. Rasetti, “Quantum Tetrahedra,” *J. Phys. Chem. A*, vol. 113, pp. 15376–15383 (2009).
- [22] R. Koekoek, P. Lesky, and R. Swarttouw, *Hypergeometric orthogonal polynomials and their q -analogues*. Springer-Verlag (2010).
- [23] T. Regge, “Symmetry properties of Racah’s coefficients,” *Nuovo Cimento*, vol. 11, pp. 116–117 (1959).
- [24] R. Littlejohn and L. Yu, “Uniform semiclassical approximation for the Wigner $6j$ symbol in terms of rotation matrices,” *J. Phys. Chem. A*, vol. 113, p. 14904–14922 (2009).
- [25] V. Aquilanti, H. M. Haggard, A. Hedeman, N. Jeevangee, R. Littlejohn, and L. Yu, “Semiclassical mechanics of the Wigner $6j$ -symbol,” *J. Phys. A*, vol. 45, no. 065209 (2012).
- [26] K. Schulten and R. Gordon, “Exact recursive evaluation of $3j$ - and $6j$ -coefficients for quantum mechanical coupling of angular momenta,” *J. Math. Phys.*, vol. 16, pp. 1961–1970 (1975).
- [27] —, “Semiclassical approximations to $3j$ - and $6j$ -coefficients for quantum-mechanical coupling of angular momenta,” *J. Math. Phys.*, vol. 16, pp. 1971–1988 (1975).